8. S. K. Hemant and K. Yates, *J. Am. Chem. Soc.* **113**, 6062 (1991).
9. The peptides, except the specifically deuterated one (see Fig. 3), were synthesized on an Applied Biosystems Model 431A peptide synthesizer with Fmoc/HBTU [9-fluorenyl methoxy carbonyl/2-(1*H*-benzotriazol-1-yl)-1,1,3,3-tetramethyluronium hexafluorophosphate] cycles [C. G. Fields, D. H. Lloyd, R. L. Macdonald, K. M. Otteson, R. L. Noble, *Peptide Res.* **4**, 95 (1991)] modified to include acetic anhydride capping. The probes are coupled to the peptides by using HBTU activation and ~30-fold molar excess of activated species to peptide-resin. Each reaction is allowed to proceed for 2 to 3 hours. The peptides (with probes attached) are cleaved from the resins by using standard Fmoc protocols, with final purification by reversed-phase high-performance liquid chromatography. The identity of the peptides with probes attached is confirmed by mass spectrometry (Mass-Search, Inc., Modesto, CA).
10. S. Marqusee, V. H. Robbins, R. L. Baldwin, *Proc. Natl. Acad. Sci. U.S.A.* **86**, 5286 (1989).
11. K. T. O'Neil and W. F. DeGrado, *Science* **250**, 646 (1990); G. Merutka and E. Stellwagen, *Biochemistry* **30**, 1591 (1991).
12. The F peptides with MABA attached have CD spectra (0°C, pH 7) typical of α helices [R. W. Woody, in *The Peptides*, S. Undenfriend, J. Meienhofer, J. R. Hruby, Eds. (Academic Press, New York, 1985), vol. 7, pp. 15–114], with minima at 222 and 208 nm. With MABA attached, $[\theta]_{222}$ for F_S and F_SR5 is −32,100 and −32,300 degree cm^2/dmol, respectively, and −39,900 and −40,600 for the longer F_L and F_LR5 peptides. $[\theta]_{208}$ for F_S, F_SR5, F_L, and F_LR5 is −25,600, −26,500, −31,400, and −32,300 degree cm^2/dmol, respectively. These CD data and measurements of GuHCl-induced unfolding of F_S with MABA attached (D. J. Lockhart and P. S. Kim, unpublished results) suggest that the 21-residue peptides are greater than 90% helical and that the 41-residue peptides are nearly 100% helical. The CD spectra of the U peptides with MABA indicate that they are unstructured. At 0°C, the CD spectrum of peptide U_S with MABA attached has a maximum of +510 degree cm^2/dmol at 227 nm and a value at 222 nm of approximately +100 degree cm^2/dmol. The CD data are obtained in a 1-cm cell with an Aviv Associates 62DS Circular Dichroism spectrometer.
13. The melting temperatures for the helical peptides, determined by the temperature dependence of the CD signal at 222 nm, are independent of peptide concentration (measured between 4 and 70 μM, and up to 4 mM for peptide F_S). The unfolded peptides have concentration-independent CD spectra at 0°C between 4 and 70 μM.
14. The probe band shift decreases by ~20% of the maximum value per molar increase in monovalent salt concentration (similar effects have been observed with NaCl, LiCl, and KF), even though salt does not affect peptide structure (<3% variation in the CD signal at 222 nm between 0 and 3 M NaCl at 0°C). The dependence of the field on ionic strength is weak probably because the helix backbone dipoles are not completely accessible to ions or solvent molecules and the dipolar field decreases rapidly with distance.
15. The observed shifts (relative to a value of 1.0 for MABA attached to F_S at 0°C) for the other probes attached to peptide F_S at 0°C are: 0.95 ± 0.05 for ABA; ≤0.3 for TPA; and −0.12 ± 0.05 for NBA.
16. K. R. Shoemaker, P. S. Kim, E. J. York, J. M. Stewart, R. L. Baldwin, *Nature* **326**, 563 (1987); D. Sali, M. Bycroft, A. R. Fersht, *ibid.* **335**, 740 (1988); H. Nicholson, W. J. Becktel, B. W. Matthews, *ibid.* **336**, 651 (1988); R. Fairman, K. R. Shoemaker, E. J. York, J. M. Stewart, R. L. Baldwin, *Proteins* **5**, 1 (1989); L. Serrano and A. R. Fersht, *Nature* **342**, 296 (1989); H. Nicholson, D. E. Anderson, S. Dao-pin, B. W. Matthews, *Biochemistry* **30**, 9816 (1991); J. Sancho, L. Serrano, A. R. Fersht, *ibid.* **31**, 2253 (1992).
17. A small degree of fraying, however, cannot be ruled out, and the probe band shift is expected to be approximately proportional to the percentage of time that the amino-terminal residues are in a helical conformation. If the amino terminus near the probe is slightly frayed [A. Chakrabartty, J. A. Schellman, R. L. Baldwin, *Nature* **351**, 586 (1991); M. I. Liff, P. C. Lyu, N. R. Kallenbach, *J. Am. Chem. Soc.* **113**, 1014 (1991); S. M. Miick, A. P. Todd, G. L. Millhauser, *Biochemistry* **30**, 9498 (1991); C. A. Rohl, J. M. Scholtz, E. J. York, J. M. Stewart, R. L. Baldwin, *ibid.* **31**, 1263 (1992)], then the electric field measured here represents a lower limit, and $\varepsilon_{\mathrm{eff}}$ is smaller than the value we have calculated.
18. D. J. Lockhart and P. S. Kim, unpublished results. The only exception is the H^P – $H^N{}_1$ crosspeak, which is expected even in the unfolded peptides.
19. A 21-residue Ala α helix is built with partial charges as assigned by the CHARMM [B. R. Brooks *et al.*, *J. Comput. Chem.* **4**, 187 (1983)] parameter set (PARAM19) and the electric field at the center of the probe is calculated by using a dielectric constant of 1. The calculated field for a 41-residue helix is larger by less than 1%.
20. M. K. Gilson, A. Rashin, R. Fine, B. Honig, *J. Mol. Biol.* **183**, 503 (1985); M. K. Gilson and B. H. Honig, *Biopolymers* **25**, 2097 (1986); M. K. Gilson and B. Honig, *Proteins* **3**, 32 (1988); D. Bashford and M. Karplus, *Biochemistry* **29**, 10219 (1990).
21. K. K. Rodgers and S. G. Sligar, *J. Am. Chem. Soc.* **113**, 9419 (1991).
22. D. C. Rees, *J. Mol. Biol.* **141**, 323 (1980); A. J. Russel and A. R. Fersht, *Nature* **328**, 496 (1987); D. Sali, M. Bycroft, A. R. Fersht, *J. Mol. Biol.* **220**, 779 (1991).
23. The sample concentration for the optical experiments is typically 15 μM. The buffer for all optical experiments contains 1 mM sodium citrate, 1 mM sodium phosphate, and 1 mM sodium borate with no added salt unless specified. The absorption data are recorded in a 1-cm pathlength cell at 0°C and pH 7, unless specified otherwise, with an Aviv Associates 14DS or 118DS spectrophotometer.
24. Two-dimensional NMR data were collected on ~4 mM samples in 100 mM sodium phosphate (pH 4.5) at 3°C. Data were collected on a Bruker AMX 500 MHz spectrometer. NOESY experiments are performed with a mixing time of 200 ms. Chemical shift is relative to TMSP [2,2,3,3-tetradeutero-3-(trimethylsilyl)-propionic acid sodium salt]. The specifically deuterated peptide is synthesized on an Applied Biosystems Model 430A peptide synthesizer using standard t-Boc/NMP (*tert*-butyloxycarbonyl/*N*-methylpyrrolidone) cycles modified to include acetic anhydride capping. t-Boc-L-alanine[3,3,3-D3] is obtained from Tracer Technologies (Somerville, MA). The peptide is cleaved with a standard t-Boc cleavage procedure (low-high trifluoromethanesulfonic acid).
25. We thank R. Rutkowski, M. Milhollen, and M. Burgess for peptide synthesis and attachment of the probes; P. Hoeprich for discussions concerning synthesis; S. Stradley for amino acid analysis; Z.-y. Peng, B. Schulman, L. McIntosh, K. Lumb, and C. J. McKnight for help with NMR; B. Tidor for help with CHARMM; B. Tidor, S. Boxer and the Kim group for discussion and critical reading of the manuscript; and D. Pierce, D. Oh, and M. Steffen for help with Stark effect measurements. D.J.L. is supported by a Damon Runyon–Walter Winchell Cancer Research Fund Fellowship. P.S.K. is a Pew Scholar in the Biomedical Sciences and a Rita Allen Foundation Scholar. This research was supported by the Howard Hughes Medical Institute.

8 May 1992; accepted 9 July 1992

The Reversal and Splitting of Waves in an Excitable Medium Caused by an Electrical Field

Hana Ševčíková, Miloš Marek, Stefan C. Müller

The reversal and splitting of traveling concentration waves was observed in a one-dimensional Belousov-Zhabotinski reaction medium under the influence of low-intensity electric field gradients (~10 V per centimeter). The wave reversal and splitting were strongly correlated with a characteristic transformation of the shape of both the wave front and the refractory tail of a wave in the local field gradient. The secondary role of generated hydrodynamic flow on wave transformation was also investigated.

Traveling waves are highly organized spatio-temporal patterns of system variables (component concentration and electrical potential) that very often underlie transmission of information, growth, and developmental processes in cells and living tissues (*1–4*) and other types of excitable systems (*5*). These wave patterns are produced because of the interaction of transport processes with the processes of ionic species production and consumption. These waves often have a relaxational character where the short excited front of a wave with a high amplitude of system variables is followed by a long refractory region with a very low amplitude. Because of this refractory region, the excitable waves cannot be reflected at the impermeable barriers, refract, or pass through each other, unlike sound or light waves. Despite this, several examples have been reported that show that under certain circumstances, the refractoriness of an excitable system can be suppressed and the phenomena similar to refraction or soliton-like behavior (*6–8*) can occur. This report describes in a semiquantitative way the mechanism of system changes that occur in the course of the reversal and splitting of a wave traveling in a capillary tube filled with a mixture that supports the Belousov-Zhabotinski (BZ) reaction and is exposed to the external electric field.

H. Ševčíková and M. Marek, Department of Chemical Engineering, Prague Institute of Chemical Technology, Technicka 5, 166 28 Prague 6, Czechoslovakia.
S. C. Müller, Max-Planck-Institut für Ernährungsphysiologie, Rheinlanddamm 201, W-4600 Dortmund 1, Germany.

An externally applied electric field can affect the velocity of propagation of concentration waves in different types of reaction-diffusion excitable media (6, 9, 10) and can control the period and the wavelength of rotating spiral waves (11, 12) and the drift of the spiral core (11) as well. Experiments on quasi–one-dimensional (1-D) BZ waves (6) have shown that the wave velocity is a nonlinear function of the electric field intensity and depends on the polarity of the field. Although the waves propagating toward the positive electrode (that is, in the negative field) are accelerated with respect to the field-free case, those moving toward the negative electrode (that is, in the positive field) are slowed down. A previous study (6) yielded qualitative evidence that the slowing down with increased positive field strength remains moderate until a critical threshold of field intensity is reached. At this critical value, wave reversal and wave splitting have been observed. We concentrated on ferroin concentration profile changes under electric field influence, specifically studying the development of the concentration profile in the course of wave reversal and wave splitting.

Wave reversal and splitting were investigated by high-resolution 2-D spectrophotometry based on a computerized video system (13, 14). To obtain an undistorted optical signal from the light transmitted through the active medium, we used a specially designed rectangular cuvette. We took measurements in both the liquid phase and the agar gel system to estimate the role of induced convective flow in the observed phenomena (15).

A typical spatial profile of the wave represented by the concentration of the oxidized form of the catalyst, ferriin, in the field-free system is shown in Fig. 1 (profile 1). The wave moves from the right to the left, converting the medium quickly from the reduced (low ferriin concentration) to the oxidized state (high ferriin concentration) and then slowly back to the reduced state. The transition to the oxidized state occurs when the bromide concentration in front of the wave is depleted as a result of chemical reactions and diffusion below a threshold value (16). This transition is fast and forms a sharp gradient of ferriin concentration. The production of the bromide starts anew in the course of the oxidation of the medium and causes the reduction process to prevail again over the oxidative one. In the course of the reduction, the initial relatively fast decrease of the ferriin concentration is followed by a slow, asymptotic approach to a stationary value, resulting in a steep wave back and a shallow refractory tail of the spatial profile. If an electric field gradient exists in the system, then in addition to diffusion the transport of species by means of selective ionic migration occurs. The local depletion of the bromide ions in front of the wave is either enhanced in a negative field or depressed in a positive field by the action of ionic migration. These effects are then reflected in either the increase or the decrease of the propagation velocity of the wave (6).

The electric field affects not only the velocity of the wave propagation but also

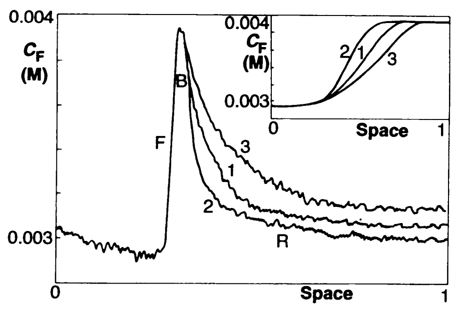

Fig. 1. Spatial profiles of the ferriin concentration C_F in the field-free system (profile 1) and in the positive (profile 2) and negative (profile 3) electric field [electric field strength (E) ≈ 8 V/cm]. Gelled system, side view. F, wave front (leading edge); B, wave back; R, refractory tail. Space unit = 12 mm. (Inset) Enlargement of the wave fronts in profiles 1, 2, and 3. Space unit = 0.6 mm.

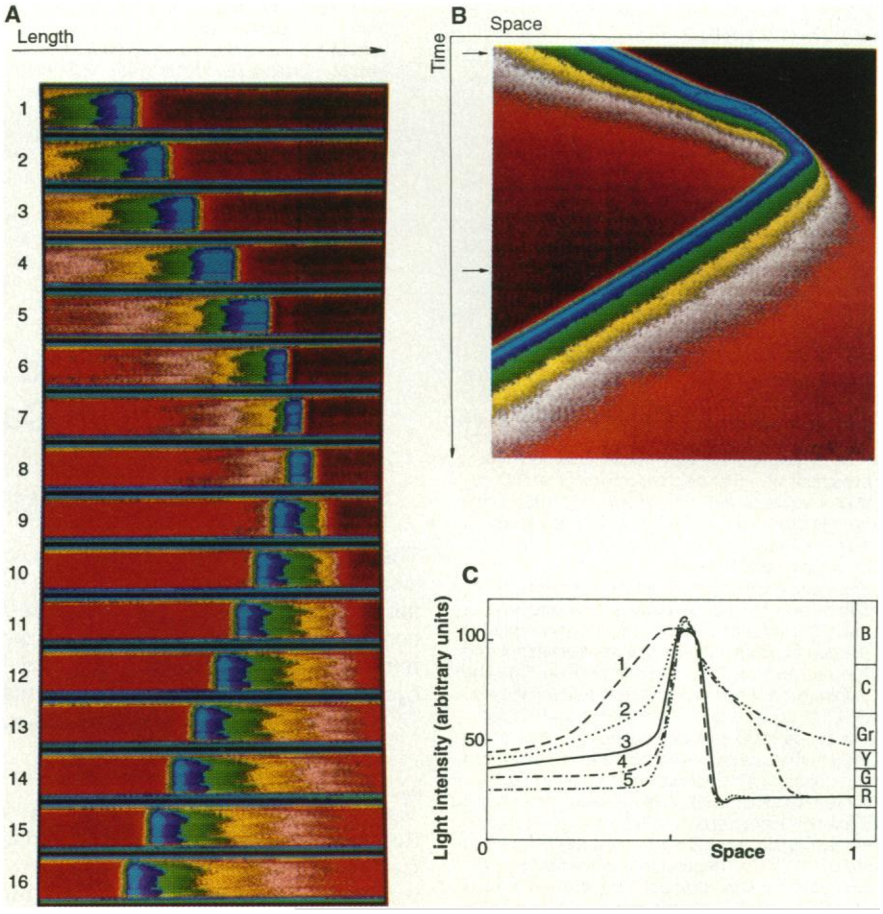

Fig. 2. Reversal of the direction of the wave propagation in the gelled system observed from the side (E ≈ 10 V/cm). (**A**) Time series of video images of the cuvette taken at 16-s intervals. In plates 1 to 3, the wave moves from the left to the right toward the anode. Between plates 3 and 4, the polarity of the field is reversed. This is immediately reflected in the enlargement of the blue zone representing the oxidized state of the medium (C). This zone than shrinks again (plates 5 to 7), and the concentration gradient of the wave back becomes steeper (the dark blue, green, yellow, and gold zones in plates 5 to 8 become narrower). In plate 7, wave back and wave front have approximately the same steepness. In plate 8, the former wave front is converted into the wave back, and the former wave back, now the wave front, starts moving backwards toward the anode. The next eight plates show the development of the wave back. Pictured length of the capillary = 6.64 mm. (**B**) Space-time plot established along the central axis of the cuvette in (A), with the same false colors. Pictured time interval = 450 s; pictured length of the capillary = 7.54 mm. Arrows mark the time interval shown in (A) in detail. (**C**) Evolution of the spatial wave profile during wave reversal. Time instants after plate 5 of (A) are: 1 = 0 s; 2 = 16 s; 3 = 40 s; 4 = 64 s; and 5 = 128 s. Space unit = 3.6 mm. The scale on the right indicates the false colors used in (A) and (B) (B, blue; C, dark blue; Gr, green; Y, yellow; G, gold; and R, red).

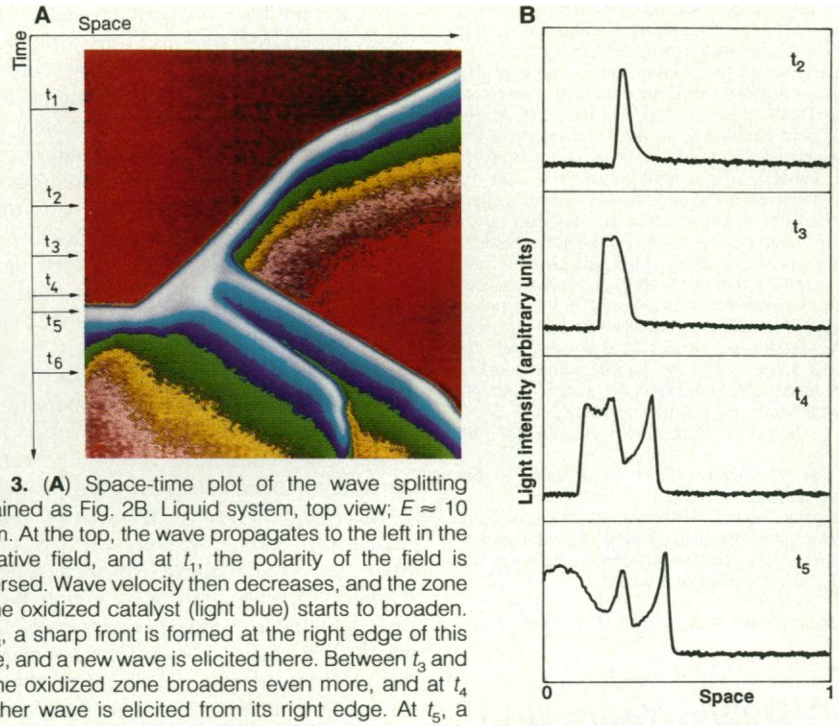

Fig. 3. (**A**) Space-time plot of the wave splitting obtained as Fig. 2B. Liquid system, top view; $E \approx 10$ V/cm. At the top, the wave propagates to the left in the negative field, and at t_1, the polarity of the field is reversed. Wave velocity then decreases, and the zone of the oxidized catalyst (light blue) starts to broaden. At t_3, a sharp front is formed at the right edge of this zone, and a new wave is elicited there. Between t_3 and t_4, the oxidized zone broadens even more, and at t_4 another wave is elicited from its right edge. At t_5, a bulk oscillation in the left portion of the cuvette annihilates the wave moving to the left. At t_6, the electric field is switched off, and the split waves slow down. After a while, the second split wave ceases to exist. Pictured length of the capillary = 11 mm; pictured time interval = 510 s. Colors are as in Fig. 2A; light blue represents the highest concentration of ferriin. (**B**) Spatial profiles of transmitted light intensity taken at times t_2, t_3, t_4, and t_5 in (A). Space unit = 17.07 mm.

the ferriin concentration profile of the wave (Fig. 1, profiles 2 and 3). Pronounced changes occur in the shapes of the wave back and of the refractory tail, whereas the shape of the wave front is almost unaffected. In the positive field, the back of the wave drops down more sharply and to a lower ferriin concentration than in the field-free system and in the negative field. Thus, the refractory tail lies under that of the zero-field wave and of the negative field wave. The wave front is focused in the positive field (that is, the concentration gradient is steeper), whereas it is slightly flattened in the negative field (Fig. 1, inset).

At a sufficiently high intensity of the positive field, wave reversal occurs, shown in Fig. 2A by a sequence of false color images. In the course of the reversal, the concentration gradient of the back of the wave becomes almost as steep and as deep as the gradient of the wave front. The migration of the bromide ions toward the anode—that is, in the direction opposite that of the wave propagation—slows the propagation of the wave front. On the other hand, it helps to decrease the bromide concentration in the refractory tail below the threshold value, and consequently the wave's trailing edge turns into a sharp wave front that moves in a direction opposite that of the original wave.

This reorganization and overturning of the wave profile during the wave reversal is shown in quantitative detail in Fig. 2C. Five profiles taken at different time instants are overlapped such that their maxima coincide. Shapes of the profiles (1 to 5) to the left of the maximum illustrate how the new wave front emerges from the wave back while the propagating wave is exposed to the critical positive field intensity. The transition of the wave front to the wave back takes place simultaneously on the right. Profiles 1 to 3 correspond to the wave moving to the right. When profile 3 is being formed, the wave almost stops and then starts to move to the left (profiles 3 to 5). Simultaneous changes of the wave front to the wave back and of the wave back to the wave front are typical.

The splitting of the wave shown in a space-time plot in Fig. 3A was observed in a number of experiments. This complex behavior depends very sensitively on the precise values of the wave velocity and of the applied field intensity. For the wave splitting to occur, it is necessary that the wave front remains when a new wave front emerges from the wave back (Fig. 3A). This is possible only if the wave front continues to move toward the negative electrode so that the wave front can reproduce itself by initiating the autocatalytic oxidation process.

As the back of the wave is transformed into the leading edge of a new wave during the process of the wave splitting and moves in the opposite direction, the zone of the high ferriin concentration (Fig. 3A) enlarges, stabilizing the oxidized state in a small portion of the medium. This region of the oxidized state forms a new source of waves (leading center) that emits waves only from the side facing the positive electrode, because both the refractoriness of the medium and the threshold conditions are more favorable for waves that propagate toward the positive rather than toward the negative electrode.

Recording the propagation of the wave and its reversal in the narrow tube both from the side and from the top confirmed that in the gelled system, these processes are in principle one dimensional, as there were no concentration gradients observed in the plane perpendicular to the longitudinal axis of the cuvette (Fig. 2A). Thus, one can conclude that only the interaction of reaction, diffusion, and migration processes is involved in the mechanism of wave reversal. Because the wave splitting was observed only in the liquid system and because experiments in the rectangular cuvette showed that vertical concentration gradients appear in the course of the wave splitting, it seems likely that fluid convection processes are also involved in wave splitting. On the other hand, this convection may not be the necessary condition for wave splitting.

No matter what particular physical and chemical processes are involved, the phenomena of wave reversal and splitting are connected to local changes in the system dynamics (changing it from an excitable to a bistable one) and to the creation of a temporal leading center. Formation of a temporal leading center was suggested to be the cause of branching observed on mollusk shell patterns, but the reason for local changes in system dynamics is still unknown (*7*). The formation of a bistable region on a defect on the Pt catalytic surface seems to provide an explanation (*17*) for the soliton-like behavior of the CO waves passing through this region (*8*). The changes of the local dynamics in our system are evoked by the interaction of the electric field of the proper intensity and polarity with the concentration gradients along the traveling wave.

REFERENCES AND NOTES

1. G. G. Matthews, *Cellular Physiology of Nerve and Muscle* (Blackwell, Oxford, 1986).
2. J. Lechleiter, S. Girard, E. Peralta, D. Clapham, *Science* **252**, 123 (1991).
3. R. Plonsey, *Bioelectric Phenomena* (McGraw-Hill, New York, 1969).
4. R. Nuccitelli, Ed., *Ionic Currents in Development* (Liss, New York, 1986).

5. A. V. Holden, M. Markus, H. G. Othmer, Eds., *Nonlinear Wave Processes in Excitable Media* (Plenum, London, 1990).
6. H. Ševčíková and M. Marek, *Physica* **9D**, 140 (1983).
7. H. Meinhardt and M. Klinger, *J. Theor. Biol.* **126**, 63 (1987).
8. H. H. Rotermund, S. Jakubith, A. von Oertzen, G. Ertl, *Phys. Rev. Lett.* **66**, 3083 (1991).
9. P. Ortoleva, *Physica* **26D**, 67 (1987).
10. H. Ševčíková and M. Marek, *ibid.* **13D**, 379 (1984).
11. O. Steinbock, J. Schütze, S. C. Müller, *Phys. Rev. Lett.* **68**, 248 (1991).
12. V. Pérez-Muñuzuri, R. Aliev, B. Vasiev, V. I. Krinski, *Physica*, in press.
13. S. C. Müller, T. Plesser, B. Hess, *Naturwissenschaften* **73**, 165 (1986).
14. _____, *Physica* **24D**, 71 (1987).
15. Experiments were performed with a modified version of the apparatus described in (*6*). A rectangular cuvette made of optically clean glass (inner cross section 0.7 mm × 0.7 mm; length 84 mm) was placed horizontally between two chambers filled with the reaction solution where the Pt plate electrodes were immersed. The entire apparatus was thermostated at 15° ± 0.2°C. We prepared the reaction mixture by mixing the proper amount of stock solutions from reagent-grade chemicals and distilled water, except for bromic acid, which was directly synthesized from $BaCl_2$, $NaBrO_3$, and H_2SO_4 (*6*). To prepare the agar gel system, we mixed the reaction solution with agar gel in the liquid state (final concentration 0.4%) and filled the cuvette with it. The concentrations after mixing were 0.201 M $HBrO_3$, 0.007 M KBr, 0.05 M malonic acid, and 4 mM ferroin. Propagating waves were investigated with a 2-D spectrophotometer. The intensity of the light beam (λ = 490 nm) passing through the cuvette was recorded with a Hamamatsu video camera and digitized by the analog-digital converter in a video frame buffer. A system of mirrors allowed the light beam to pass the cuvette either horizontally or vertically to estimate the one-dimensionality of the wave propagation. The maximal magnification corresponded to a space resolution of 18 mm per pixel. The waves traveling into the cuvette were produced spontaneously at the inlet holes where the cuvette is attached to the solution chambers.
16. R. J. Field and R. M. Noyes, *Nature* **237**, 390 (1972).
17. M. Bär, M. Eiswirth, H.-H. Rotermund, G. Ertl, *Phys. Rev. Lett.*, in press.
18. We thank I. Beyer, S. Kohaupt, O. Steinbock, and A. Warda for their help with the technical aspects of the experiments, D. Dopitova for drawings, and G. Schulte for color photographs.

19 March 1992; accepted 16 June 1992

Coeval ^{40}Ar/^{39}Ar Ages of 65.0 Million Years Ago from Chicxulub Crater Melt Rock and Cretaceous-Tertiary Boundary Tektites

Carl C. Swisher III, José M. Grajales-Nishimura,
Alessandro Montanari, Stanley V. Margolis, Philippe Claeys,
Walter Alvarez, Paul Renne, Esteban Cedillo-Pardo,
Florentin J-M. R. Maurrasse, Garniss H. Curtis,
Jan Smit, Michael O. McWilliams

^{40}Ar/^{39}Ar dating of drill core samples of a glassy melt rock recovered from beneath a massive impact breccia contained within the 180-kilometer subsurface Chicxulub crater in Yucatán, Mexico, has yielded well-behaved incremental heating spectra with a mean plateau age of 64.98 ± 0.05 million years ago (Ma). The glassy melt rock of andesitic composition was obtained from core 9 (1390 to 1393 meters) in the Chicxulub 1 well. The age of the melt rock is virtually indistinguishable from ^{40}Ar/^{39}Ar ages obtained on tektite glass from Beloc, Haiti, and Arroyo el Mimbral, northeastern Mexico, of 65.01 ± 0.08 Ma (mean plateau age for Beloc) and 65.07 ± 0.10 Ma (mean total fusion age for both sites). The ^{40}Ar/^{39}Ar ages, in conjunction with geochemical and petrological similarities, strengthen the recent suggestion that the Chicxulub structure is the source for the Haitian and Mexican tektites and is a viable candidate for the Cretaceous-Tertiary boundary impact site.

The global search for an impact crater of sufficient size to account for the extinctions at the close of the Cretaceous period has focused recently on a subsurface circular structure, 180 km in diameter, centered at Chicxulub on the north coast of the Yucatán Peninsula (*1*, *2*) (Fig. 1). If an impact origin is confirmed, the Chicxulub structure, whose outline is based on circular magnetic and gravity anomalies, will be the largest impact crater yet found on Earth. Its size and the proximity to abundant tektites and microtektites recovered in marine Cretaceous-Tertiary (K-T) deposits near Beloc, Haiti (*3–5*), and at Arroyo el Mimbral in northeast Mexico (*6*) and to proximal wave deposits of probable tsunami origin in the Gulf of Mexico (*6*, *7*) make the Chicxulub structure an ideal candidate for the K-T impact site that triggered the mass extinctions at the close of the Cretaceous period.

The stratigraphy of the Chicxulub structure is known primarily from a transect of petroleum exploration wells drilled across the Yucatán Peninsula by Petróleos Mexicanos (PEMEX) (*8–10*) (Fig. 1). Three of these wells, Yucatán 6 (Y-6), Chicxulub 1 (C-1), and Sacapuc 1 (S-1), occur within the Chicxulub geophysical anomaly. These wells penetrated marl and limestone underlain by coarse breccia, polymict breccia, and glassy rocks of andesitic composition. The polymict breccia is composed of a mixture of microcrystalline crystals of alkali and plagioclase feldspar, pyroxene (augite), rounded and angular quartz, and minor amounts of euhedral zircon, barite, and Ti-Fe oxides. The angular quartz grains appear to be etched and show multiple sets of planar lamellae indicative of shock metamorphism. The underlying unit is composed of angular pyroxene (augite) crystals embedded in a glassy or microcrystalline groundmass of alkali and plagioclase feldspars. These andesitic glasses and microcrystalline rocks are interpreted as impact breccias and melt rocks of andesitic composition (*2*). Earlier workers (*8*) concluded that the breccia above the melt rocks is Upper Cretaceous in age, which would indicate that the impact age is older than the K-T boundary. However, other workers have estimated on the basis of poorly preserved foraminifera that the rocks are as young as early Paleocene (P3) (*11*). A plausible explanation for the occurrence of Cretaceous deposits above the melt rocks is that they represent fallback breccia of Cretaceous limestone infilling a crater of K-T age. The uncertainty in the age of the Chicxulub crater makes radioisotopic dating of the melt rock imperative.

The possibility that the Chicxulub structure is the source for the Haitian and Mexican tektites has recently been strengthened by chemical analyses of the microcrystalline melt rocks recovered from Yucatán 6 (*2*) (Table 1). The composition of the andesitic melt rock is clearly within range of that observed for the Haitian and Mimbral tektites; and the limestones of the Yucatán Platform can explain the more Ca-rich tektites (*4*, *6*). Detailed microprobe analyses of the glassy feldspathic groundmass from sample C-1 (Fig. 1 and Table 1) from the Chicxulub 1 well indicate that it is andesitic in composition and

---

C. C. Swisher III, P. Renne, G. H. Curtis, Geochronology Center, Institute of Human Origins, 2453 Ridge Road, Berkeley, CA 94709.
J. M. Grajales-Nishimura and E. Cedillo-Pardo, Instutito Mexicano del Petróleo, Eje Central Lazaro Cardenas No. 152, 07730 México D. F., México.
A. Montanari and W. Alvarez, Department of Geology and Geophysics, University of California, Berkeley, CA 94720, and Osservatorio Geologico, Col di Gioco, Apiro (MC), Italy.
S. V. Margolis and P. Claeys, Department of Geology, University of California, Davis, CA 95616.
F. J-M. R. Maurrasse, Department of Geology, Florida International University, Tamiami Trail and Southwest 107th Avenue, Miami, FL 33199.
J. Smit, Department of Sedimentary Geology, Free University, de Boelelaan 1085, 1081HV Amsterdam, Netherlands.
M. O. McWilliams, Department of Geophysics, Stanford University, Stanford, CA 94305.